Baxter, D., Perry, S. R., Hill, T. A., Kok, W. M., Zaccai, N. R., Brady, R. L., Fairlie, D. P., & Mason, J. M. (2017). Downsizing proto-oncogene cFos to short helix-constrained peptides that bind Jun. *ACS Chemical Biology*, *12*(8), 2051-2061. https://doi.org/10.1021/acschembio.7b00303

Downsizing protooncogene cFos to short helix-constrained peptides that bind Jun

Daniel Baxter[1†], Samuel R. Perry[2†], Timothy A. Hill[2], W. Mei Kok[2], Nathan R. Zaccai[3], R. Leo Brady[3], David P. Fairlie[2] & Jody M. Mason[1*]*

[1]Department of Biology & Biochemistry, University of Bath, Claverton Down, Bath, BA2 7AY, UK

[2]Division of Chemistry and Structural Biology, Australian Research Council Centre of Excellence in Advanced Molecular Imaging, University of Queensland, Brisbane, Queensland 4072, Australia

[3]School of Biochemistry, University of Bristol, University Walk, Bristol BS8 1TD, UK

[†]Joint first authors

*Corresponding authors: Prof David Fairlie (E: d.fairlie@uq.edu.au; T: +61733462989) and Dr Jody M. Mason (E: j.mason@bath.ac.uk; T: +441225386867)

Keywords: Coiled coil; Activator Protein-1; helix-constrained peptide; transcription factor

The oncogenic transcription factor Activator Protein-1 (AP-1) is a DNA binding protein that assembles through dimerization of Fos and Jun protein subunits, their leucine-rich helical sequences entwining into a coiled coil structure. This study reports on downsizing the protooncogene cFos protein (380 residues) to shorter peptides (37-25 residues), modified with helix-inducing constraints to enhance binding to Jun. A crystal structure is reported for a 37-residue Fos-derived peptide (FosW) bound to Jun. This guided iterative downsizing of FosW to shorter peptide sequences, constrained into stable water-soluble alpha helices by connecting amino acid sidechains to form cyclic pentapeptide components. Structural integrity in the presence and absence of Jun was assessed by circular dichroism spectroscopy, while thermodynamics of binding to cFos was measured by isothermal titration calorimetry. A 25-residue constrained peptide, one-third shorter yet 25 % more helical than the structurally characterised 37-residue Fos-derived peptide, retained 80 % of the binding free energy due to pre-organisation in a Jun-binding helix conformation, with entropy gain (TΔS = + 3.2 kcal/mol) compensating for enthalpy loss. Attaching a cell penetrating peptide (TAT_{48-57}) and a nuclear localisation signal (SV40) promoted cell uptake, localisation to the nucleus, and inhibition of the proliferation of two breast cancer cell lines.

INTRODUCTION

Most biological functions are mediated by protein-protein interactions (PPIs), often involving large protein surface areas and shallow binding interfaces that are not conducive to targeting with conventional drug-like small molecules. An alternative approach under intensive investigation is to downsize one of the interacting protein surfaces, often a helix, to a bioactive small peptide capable of functionally mimicking or antagonizing the PPI [1]. Short peptide sequences do not form thermodynamically stable helices in water. However, amino acid variations based on known α-helical propensities [2], together with incorporating helix constraints, can realise potent peptidic and peptidomimetic antagonists of PPIs [1, 3], and some efficacious peptides have entered clinical trials [4]. The helix constraints pre-organise peptides in receptor-binding α-helical conformations [5], with improved protein-binding affinities [6], protease resistance [7-8] and, in some cases, increased cellular uptake [6]. Lactam bridges have been shown to be the most effective constraints for inducing peptide α-helicity [9]. Appropriately placed constraints have been shown to induce helicity and compensate for loss of enthalpy and binding free energy normally associated with considerable truncation[5]. They have been used in conjunction with peptide truncation to derive small helical peptides that penetrate cell membranes [10]. Helix constraints can therefore compensate for the loss of binding free energy, associated with shortening peptide sequences, by pre-organizing peptides to minimize the entropic penalty for rearranging to a protein-binding helical conformation [5].

Activator Protein-1 (AP-1) is a dimeric transcription factor that is hyperactivated in tumourigenesis [11-12] and therefore antagonism of its function represents a promising therapeutic strategy for a number of human cancers [13]. AP-1 consists of different sub-units that are assembled via a bZIP domain. This is composed of a DNA-binding basic region and a 'leucine zipper' region involving a supercoiled heterodimer region of Jun (cJun, JunB, JunD) and Fos (cFos, FosB-1 and 2, Fra-1 and 2) proteins [14]. The Jun-Fos coiled coil binding interface features pseudo-parallel alignments of α-helical segments of Jun and Fos that make contacts over the length of the helices [15]. This PPI is difficult to target with hydrophobic drug-like molecules due to the lack of well-defined hydrophobic pockets [16] and to the difficulty in discriminating between the two interacting helical segments of Jun and

Fos proteins. Small molecules examined to date have lacked Jun/Fos specificity [17-18], which is essential given that some AP-1 compositions have been shown to be anti-oncogenic [12].

AP-1 can be antagonised by cJun mutants that lack transactivation domains [19-20], by cJun and cFos mutants with truncated DNA-binding domains [21], and by mutations in DNA-binding domains that then require an extended dimerisation interface [22]. These mutant peptides bind efficiently to Jun and, when expressed in cells, can inhibit AP-1 to cause cell cycle arrest and reduced cell proliferation [22-24]. However, such polypeptides are susceptible to degradation by proteases, do not permeate cell membranes, and have low bioavailability. Here we investigate the possibility of deriving short helical peptides from the Jun-binding region of cFos, a protein consisting of 380 amino acid residues featuring a leucine zipper region for heterodimerisation with Jun, a basic region for binding to DNA, and a transactivation domain at its C-terminus. We report steps towards minimising the length of the Fos fragment, altering it using helix constraints to optimise Fos-Jun interactions, and modifying the peptides further for entering cancer cells and targeting AP-1 in the nucleus to inhibit proliferation. This minimalist approach using helix constraints is still an under-utilised strategy for modulating protein-protein interactions, but it is unclear whether it can be useful in producing effective antagonists of protein-protein interactions specifically involving coiled coils that tend to involve key interactions along their entire interface [25].

RESULTS

Structure of FosW-Jun, a model protein-protein interface

We have previously used an intracellular protein-fragment complementation method [26] to derive a 37-residue peptide FosW [27] from a cFos-based library. This peptide was able to bind Jun and antagonise both Fos-Jun and Jun-Jun protein-protein interactions, but the structure of FosW-Jun is unknown. Here we have complexed FosW with Jun, obtained diffracting crystals, and determined a crystal structure to a resolution of 2.3 Å (Figure 1 and Table S1) (PDB ID: 5fv8). This is the first crystal structure of an AP-1 antagonist in complex with its target, and importantly identifies the anticipated binding mode of FosW with Jun [26].

Inspection of the crystal structure shows that FosW and Jun have bound together to form a parallel dimeric coiled coil, with characteristic hydrophobic interactions (***a***$_i$-***a'***$_i$ and ***d***$_i$-***d'***$_i$) and electrostatic contacts (***g***$_i$-***e'***$_{i+7}$ and ***e***$_i$-***g'***$_{i-7}$) (Figure 1 and Supplementary Information). Consistent with other coiled coils [3], all ten residues at positions ***a*** and ***d*** are appropriately aligned for burying hydrophobic side chains away from the water solvent. This confers a major energy contribution to dimerisation [28], with interatomic distances consistent with important structure-stabilising interhelical ***a***-***a'*** and ***d***-***d'*** interactions [15, 29]. Thus our selection of predominantly bulky hydrophobic side chains to substitute at positions ***a*** of FosW has evidently improved sidechain packing in the core relative to cFos residues (TΔL, TΔI, KΔN and KΔL), thereby increasing enthalpy and driving dimerization.

Interactions between ***g***1 E and ***e'***2 K, and ***g***3 E and ***e'***4 R are potentially helix-stabilising. Residues at ***g***2, ***e'***3, ***e***3, ***g'***2, ***e***4 and ***g'***3 are correctly positioned to make similar interhelical interactions, but are too far apart to form contacts. Finally, an anticipated ***e***2–***g'***1 E–K interaction is not present in the crystal structure; rather the ***g'***1 K amine nitrogen faces away from the ***e***2 E. The crystal structure indicates that ***g***2 R interacts with solvent rather than with ***g***3 E. The ***e***4 E does not interact with ***g'***3 T, but may shield FosW ***a***4 I from solvent with its hydrocarbon chain. Similarly, ***e***1 and ***g***4 Q residues, which have no ***g'***$_{i-7}$ or ***e'***$_{i+7}$ partner, shield ***a***2 I and ***d***4 L core residues. Finally, we note that positions ***b***, ***c*** and ***f*** are occupied by residues that are not significantly involved in interhelical interactions according to the crystal structure, instead appearing to be involved in solvent interaction for solubility. Possible exceptions may be intrahelical interactions, such as a proposed salt bridge between ***f***3 K and ***b***4 E, with attraction of ***f***4 K towards the ***b***4 E and a cation–π attraction between ***b***3 Y and ***f***3 K. The contributions of these intrahelical interactions to α-helix adoption and dimerisation free energies are, however, expected to be small. As such, FosW ***b***, ***c*** and ***f*** positions may tolerate replacement residues that form helix constraints without significantly affecting the PPI interface [26].

Jun is predicted to be a more attractive target than Fos because of a more typical and hydrophobic interface at ***a*** and ***d*** positions of the Jun heptads (Figure 1) compared to the polar T/K-containing Fos core [26-27]. As a consequence, Fos is reported to be unable to form homodimers, and requires Jun family members to form transcriptionally active heterodimers [30]. Complexes containing Jun are also more potent for transcriptional

transactivation [30], and Jun has been implicated in a number of cancers [11-12], making antagonists of this particular homologue potentially valuable. Therefore, we have concentrated here on downsizing Fos rather than Jun to create antagonists of the Fos-Jun protein-protein interaction.

Downsizing FosW via helix-inducing constraints

The major aim was to introduce one or more helix-inducing constraints into the FosW sequence to enable downsizing of the molecule while maintaining helicity and ultimately affinity for cJun. All helix-constrained peptides lacked five residues that served as N-terminal and C-terminal capping motifs within the FosW parent peptide. This led us to iteratively examine the effect on helix induction and affinity using one or more such constraints placed at different positions within the sequence, while concomitantly truncating the sequence from either terminus (see Figure 2 and Supplementary Information).

An (*i*→*i*+4) lactam bridge was first incorporated at different positions along the sequence to learn which heptad regions were most amenable to modification with a helix-inducing constraint. This was achieved by cross-linking two amino acid residues at positions shown to have minimal involvement in Fos-Jun interhelical interactions in the crystal structure, namely ***b***-to-***f*** or ***f***-to-***c*** in the heptad repeat units of FosW (Figure 2, compounds **1-5 and Figure S1**). Compounds **1** and **3** had similar helicity (44 % and 40 %) to FosW (41 %), while compounds **2**, **4** and **5** were more alpha-helical (62 %, 59 %, 79 % respectively). However, only compounds **1** and **2** showed higher binding affinity for Jun (K_d 9.6 nM, 16.2 nM) relative to FosW (K_d 39 nM), whereas **4** and **5** had binding comparable to FosW (K_d 40 nM and 29 nM). Compound **3** did not display any affinity for Jun indicating that crosslinking at those positions was unproductive.

Since **1** had the highest binding affinity, a lactam bridge crosslinking residues K29-D33 was retained in compounds **6-9** (Figure 2), which also contained a second bridge between residues 4-8, 8-12, 15-19 or 23-26 to further increase helicity (53 %, 85 %, 78 % and 82 %) over the moderately helical compound **1** (44 %). Compounds **7**, **8**, and **9** retained affinity for Jun (K_d 8.6 nM, 9.9 nM and 11 nM) while **6** had slightly less affinity. Since **7-9**

retained affinity (K_d <10 nM) and had high helicity (>70 %), the constraints used in these compounds became the focus of our efforts to downsize FosW.

Neither 22-residue peptides **10** and **11**, with lactam bridges at positions 15-19, 22-26 and 29-33, nor the same length peptides **12** and **13** with lactam crosslinks from positions 8-12, 15-19 and 22-26 (**12-13**), were able to bind to Jun (trance did not exceed the non-interaction average or displayed low T_m values), and only **10** had helicity above 40 %. Extending the N-terminus to 25 residues, while incorporating a lactam crosslink at positions 22-26 gave **14-15,** with K_d 2.2 μM and 1 μM respectively. Removing the 22-26 bridge resulted in loss of binding affinity. Compound **15** was highly alpha helical (65 %). Shortening the peptide to 22 residues (**17**) abolished affinity for Jun.

In an effort to restore binding affinity, the sequence length was extended to 29 residues. Compounds were truncated from the N-terminus and lactam bridges inserted at positions 7-11 and 29-33 (**18**), or 11-15 and 29-33 (**19**). These compounds had significant binding affinity (K_d = 56 nM and 100 nM) and helicity (72 % and 64 %). Subsequent truncation from the N-terminus of **19** to 25 residues gave compound **20** with higher affinity (K_d 2 μM) and alpha helicity (85 %) (Figure S1).

Having identified some shorter peptides, isothermal titration calorimetry (ITC) (Figure 3 and Figure S2) was used to assess enthalpic and entropic energy contributions to binding to Jun (Table 1). Compounds **14** and **15** had the highest negative entropy of binding ($T\Delta S$ = -5.7 and -5.2 kcal per mol), while peptides **18**-**20** had improved ΔG retention. The 25mer peptide **20** retained substantial binding free energy through entropic gain and was a good compromise between shortening the sequence (reducing enthalpy) and constraining the helix (increasing entropy).

Helicity is expected to be an important contributor to binding affinity [2, 5]. Interacting peptides had homomeric helicities ≥ 39 % with a mean helicity (63 %) substantially higher than for FosW (41 %), whilst non-interacting peptides had a mean helicity of 37 %, close to that of FosW. When mixed with Jun, interacting peptides had heteromeric helicities ≥44 % with a mean helicity (55 %), much higher than FosW–Jun (37 %), whilst non-interacting peptides had a mean helicity of 26 %. However, contrary to expectations, there were no

strong relationships between helicity, affinity and entropy beyond these qualitative thresholds (See Supplementary Information).

Peptide 20 binds Jun effectively via entropic pre-organisation

Peptide **20** consists of a NΔ9CΔ3 peptide (loss of 9 residues from the N-terminus and 3 from the C-terminus relative to FosW; Figure 2) and can make 8 ***a***/***d*** and 2 ***e***/***g*** favourable interactions with Jun, compared with 10 ***a***/***d*** and 3 ***e***/***g*** favourable interactions for FosW binding to Jun. It also produced coiled coils with Jun that were much more helical (62 %) than FosW–Jun (37 %) (Figure 3). The increased helicity can be attributed to the two helix constraints positioned at the N- and C-terminus. Therefore despite truncation of one-third of the sequence relative to FosW, significant binding energy was maintained. Furthermore, **20** displayed the expected entropy benefit conferred by the two helix constraints, a significant gain of +3.2 ± 0.5 kcal/mol to TΔS compared to FosW–Jun (Figure 3), thereby compensating for a loss of enthalpy accompanying the sequence shortening from FosW. Peptide **20** demonstrated that the N-terminus of FosW is not absolutely required for Jun interaction, and that N-terminal truncation is possible with correct placement of helix-inducing constraints. The success of peptide **20** is striking when comparing the helicity of **20**–Jun (62 %) with the unconstrained counterpart, LIN20–Jun (38 %). The latter is comparable to that of FosW–Jun (37 %) but, in contrast, displayed insignificant heterodimerisation compared to either dimer as measured by thermal denaturation experiments (Figure 3). As a result, the binding of **20** to Jun (K_d 2.0 ± 0.0 μM) is almost 30-fold greater than for LIN20 (K_d ≈ 55 μM) (Figure 3).

Development of cell permeable compounds

Compounds **18** (29 residues) and **20** (25 residues) were identified as compromises between truncating the peptide sequence and retaining some of the affinity observed for FosW (37 residues) binding to Jun. To investigate whether these peptides would enter cells, fluorescein isothiocyanate (FITC) was coupled to their N-terminus via a flexible linker (6-aminohexanoic acid) to allow detection via flow cytometry and live cell confocal microscopy. There was negligible uptake of either FITC-**18** or FITC-**20** into MCF-7 breast cancer cells after

1 h or 6 h (Figure 4B). Thus, further modification of these peptides to promote cell uptake or penetration was needed if these compounds were to exhibit biological activity in cells. Three strategies were investigated for delivering these helix-constrained peptides into cells: attaching a lipid, appending a cell penetrating peptide (CPP) sequence, or replacing the polar helix-constraining lactam bridges with more hydrophobic helix-constraining hydrocarbon linkers.

Firstly, palmitic acid was conjugated to the N-terminus of peptide **20** to give Pal-**20**, anticipated to interact with the lipid bilayer to enhance uptake [31]. However, the conjugate showed no significant binding to Jun, as measured by CD or ITC techniques. Secondly, the first ten residues of cationic cell penetrating peptide sequence TAT derived from HIV-1 [32] was attached to the C-terminus of **20** to give **20-**TAT_{48-57}**,** but this is only known to enhance peptide uptake into the cytoplasm, not the nucleus. An additional nuclear localisation signal sequence from the SV40 large T-cell antigen [33] was therefore also appended to produce **20**-NLS-TAT_{48-57}, for the purpose of both enhancing cell uptake and directing **20** to the nucleus. These peptide appendages did not significantly affect binding affinity for Jun, and a positive TΔS term was maintained (Table 1). The third strategy involved replacing the lactam bridges in compounds **18** and **20** with more hydrophobic hydrocarbon bridges to give 18-HC and 20-HC, which was found to reduce binding affinity for Jun (K_d 320 nM and 15 μM, respectively) but maintain a positive TΔS term (Table 1).

Cell uptake was monitored by flow cytometry using FITC labelled analogues of **18**HC, **20**HC, **20**-TAT_{48-57} and **20**-NLS-TAT_{48-57} (Figure 4B). **20**-NLS-TAT_{48-57} showed the highest cell uptake with the most fluorescence at 1h and 6 h, comparable to FITC-labelled TAT_{48-57} alone. Cells incubated with **20**-TAT_{48-57} displayed increased levels of fluorescence at 6h, whilst **18**HC and **20**HC had comparable levels of cell uptake after 6 h. We next analysed these peptides by live cell confocal microscopy to observe how these compounds were distributed throughout the cell. FITC-**18**HC and FITC-**20**HC localised differently within MCF-7 cells. FITC-**18**HC was freely distributed throughout the cytosol and the nucleus, whereas FITC-**20**HC was mainly trapped within endosomes or aggregated within the cell (Figure 4B), possibly owing to a change in the net charge of the protein (-4 vs -2). TAT_{48-57} (FITC-**20**-TAT_{48-57}) showed cytosolic uptake and a small amount of nuclear localisation. However, addition of the nuclear localisation signal (FITC-**20**-NLS-TAT_{48-57}) promoted very efficient cellular uptake

and led to much greater nuclear localisation. All four compounds were distributed differently in the cells, potentially impacting on their biological properties.

Antiproliferative activity in human breast cancer cells

Both MCF-7 and ZR75-1 are breast cancer cell lines that are dependent on AP-1 activity for proliferation [34-35]. Having demonstrated that C-terminal appendage of cationic cell penetrating peptides was sufficient to facilitate efficient cellular uptake and nuclear localisation of **20,** or alternatively that hydrocarbon staples were sufficient to facilitate cell uptake and nuclear localisation of **18**, we next sought to investigate whether these peptides inhibited cell proliferation. Treatment with **20**, **20**HC, **18** or **18**HC did not affect proliferation of MCF-7 or ZR75-1 cells at the concentrations tested (Figure 4C, 4D). However, **20**-TAT_{48-57} did significantly reduce proliferation of both MCF-7 (83 % reduction) and ZR75-1 cells (70 % reduction) at 30 μM, while **20**-NLS-TAT_{48-57} at the same concentration reduced proliferation to an even greater extent (95 % and 96 % respectively, Figure 4D). Neither TAT_{48-57} nor NLS-TAT_{48-57} alone at the same concentration reduced cell viability (Figure 4C, 4D), and no peptide showed any haemolytic activity on red blood cells after six hours at peptide concentrations up to 30 μM, indicating that cell viability was not inhibited by the peptides through non-specific membrane disruption (Table S2).

These results indicate that our successful strategy of downsizing Fos to helix-constrained short peptides has overcome the energy barrier to binding Jun. The next hurdle was to modify the short peptide antagonists for cell uptake and nuclear localisation. Cell uptake was achieved by making the helix constraints more hydrophobic, but a nuclear localisation signal was still required to access the intracellular target of Fos peptides and affect proliferation of AP-1 containing breast cancer cells. These important steps taken here to target the Fos-Jun binding interface provide a valuable platform for further development of Fos-derived small molecules as AP-1 inhibitors in cancer therapy.

DISCUSSION

Helix constraints confer affinity to cFos peptides enabling their shortening

The 37-residue truncated analogue of cFos (FosW) has been crystallised here in complex with a Jun peptide. FosW is an antagonist of the interaction of Jun with Fos [26]. The crystal structure of FosW-Jun has identified the relative positioning of amino acid sidechains in FosW and Jun and their specific involvement in inter-helix interactions that stabilise the heterodimer in a coiled-coil complex (Figure 1). The structure provides valuable information as to the optimal sites for modifying Fos without disrupting interhelical interactions. Nevertheless, truncating this peptide was found to substantially attenuate binding affinity for Jun, due principally to loss of binding enthalpy, as demonstrated by the linear counterpart of **20** (LIN20) (Table 1). To compensate for this loss of enthalpy upon truncating the FosW sequence, we have investigated the effect of incorporating one, two or three helix-inducing (*i*→*i*+4) lactam bridges at positions in FosW away from the helix-helix binding interface with Jun. These constraints were anticipated to reduce the conformational entropic penalty for helix formation [36]. Promotion of helicity was anticipated to improve binding affinity for Jun, which is dependent on a supercoiling event between helical partners [2, 37-38]. By increasing helicity in truncated FosW analogues, we anticipated reducing the entropic penalty associated with pre-organising the shortened helix for target binding, a strategy used successfully to enable downsizing of other α-helical partners in protein-protein interactions [5-6, 39].

Lactam helix-inducing constraints at (*i*→*i*+4) positions were chosen due to their ability to impart greater alpha helicity per residue relative to other linkers, such as hydrocarbons, triazoles, *m*-xylene thioether and alkyl thioether [9], and due to the simplicity and minimal sequence disturbance of merely connecting amino acid sidechains to form lactams. Positioning these cyclic pentapeptide motifs within the FosW sequence induced substantial α-helicity (60-77 %) relative to the linear sequence, despite significant shortening. However, we find here that high helicity alone in Fos peptide analogues does not guarantee high affinity for Jun (See Supplementary Information), reinforcing the importance of sequence in coiled coil formation and stability. The use of helix constraints was anticipated to permit at least some truncation of the FosW sequence without loss of Jun binding. Indeed, truncation from either terminus coupled with careful positioning of the helix-inducing constraints between non-interfacial ***b***, ***c*** and ***f*** residues, particularly at peptide

termini, has successfully enabled identification of truncated peptides which maintain both high helicity and affinity for Jun (Figure 2, 3).

Compounds **18** (29 residues, K_d 56 nM) and **20** (25 residues, K_d 2 μM) were identified as compromises between shortening the peptide sequence (22 % and 33 %, respectively) relative to FosW and retaining some of the affinity observed for FosW (37 residues) binding to Jun. Additionally, **18** and **20** retained high helicity (69 % and 62 %, respectively) when bound to Jun (15 % helical in isolation[27]), compared with 72% and 85% in isolation (i.e. homodimeric – see Figure S2). For **20** there was a clear entropic gain that contributed to the favourable interaction free energy, and this partially compensated for a loss in binding enthalpy. Conversely, LIN20 suffered the same enthalpic loss as **20** (within 1.1 kcal/mol), but without constraints there was no entropy gain, and so ΔG was reduced by 43 % compared to FosW. The helix-inducing constraints in **20** therefore provide 19 % of the free energy of binding compared to the unconstrained peptide, translating to a 27-fold improvement in affinity for Jun. This finding demonstrates the value of helix-inducing constraints in truncated peptides for maintaining significant bioactivity. These two peptides show greater ligand efficiency (ΔG per unit molecular weight), higher entropy gain, and greater water solubility than similar length analogues, **14** and **15**. Peptides **20** and **18** were therefore chosen for the next stage, the testing of cellular uptake and functional activity.

Helicity, entropic stabilisation and binding affinity

Helix-inducing constraints are expected to confer an entropy advantage by pre-organising peptides in the helix-binding conformation preferred by the target. Molecules with greater helicity might better form coiled-coils [5, 37-38], however we find this to be an over-simplification. For the case of a coiled coil, there is likely a limit to the entropy value of pre-organising a helical structure. Above a certain threshold helicity, conformational entropy may oppose coiled-coil formation [27], perhaps reflecting a need for flexibility in a helix to enable some distortion necessary for supercoiling [40-41]. A key issue with a coiled-coil is that there is usually a fairly even contribution of residues along the entire coil to the binding energy, with fewer hot spots localised in a single region of the sequence that can form the basis for truncation. It is notable that truncation to **20** results in substantial loss of

enthalpy, consistent with enthalpy contributions from residues all along the coiled coil [5]. This may prevent further antagonist truncation, requiring innovation to increase both entropy and enthalpy through unnatural amino acid replacements that still enable coiled coil formation. Consequently, very few short helical antagonists of coiled coil PPIs have been described in the literature to date [25].

Cell uptake and nuclear localisation

AP-1 is localised in the cell nucleus, so the development of Fos-derived peptides that can antagonise Fos-Jun binding is only the first step towards drugs that can modulate AP-1 *in vivo*. The unconstrained and polar FosW peptide antagonist of Jun–Fos binding has low conformational stability, high susceptibility to degradation by proteases in blood and in cells, and poor permeability across cell membranes. Helix constraints have been found to improve all of these properties for some peptides [5-6]. However, cellular uptake is difficult to predict. It is highly dependent on the peptide sequence, the type of helix constraint, and the cell type [42].

Given the size of our short FosW-derived peptides compared to cellular Jun and Fos proteins, it was our aim to assess their ability to compete with these for an interaction with Jun inside the cell. We chose **20** for assessment of cellular uptake and nuclear localisation because of its higher affinity (K_d 2 μM) compared to the shortest Jun-derived antagonist of Jun-Fos interactions (K_d 7.3 μM) reported previously [5], and the greater expected value of Fos-peptides as antagonists against oncogenic Jun [11-12, 30] than for Jun-peptides against cFos [5]. While lactam-bridges were very effective as helix-inducing constraints in FosW-derivative peptides, there was no evidence for cell internalisation of **20**. Previous reports of the cell penetrating potential of hydrocarbon constrained peptides [42] encouraged the synthesis of the analogue FITC-**20**HC. While that peptide did pentrate cells, it did not display favourable intracellular distribution for AP-1 targeting. The longer peptide analogue **18**HC, which also had higher affinity for Jun than **20**HC, was also generated to compare cellular uptake and activity. Cell uptake did increase, but there was little uptake into the nucleus and consequently the peptide concentration may not have been high enough for AP-1 inhibition. We therefore added TAT_{48-57} or a NLS-TAT_{48-57} appendage to help drive higher cell uptake

and target more **20** to the cell nucleus where AP-1 is active (Figure 4). TAT_{48-57} increased uptake and favourable distribution, which further increased with additional inclusion of the NLS sequence (Figure 4). Considering the minimal concentrations (μM) known to be required for internalisation of cationic CPP conjugates [43], these conjugates of **20** were considered to have been delivered at a minimum effective concentration. Cytoplasmic co-translational/post-translational sequestration of Jun before nuclear transport may also be desirable to expedite Jun degradation by cytoplasmic ubiquitin/proteasomal pathways. Thus, the improved nuclear and cytosolic presence of **20**-NLS-TAT_{48-57} over **20**-TAT_{48-57} was considered to be promising for AP-1 inhibition.

Antiproliferative activity of 18 and 20 in breast cancer cells

AP-1 is known to be overexpressed in many breast cancers [44], where it drives tumour initiation and development [45], and thus is an important target for cancer therapy. MCF-7 and ZR75-1 breast cancer cells are dependent on AP-1 for expression of a variety of genes in response to pro-oncogenic growth factors [34], including extracellular matrix metalloproteinase MMP9 [46-47] and G1→S phase regulator Cyclin D1 [24, 35], such that reduced metastatic potential and cancer cell proliferation results from repression of these genes. Poor uptake, endosomal trapping and/or aggregation, and low Jun binding affinity may have prevented **20**HC from affecting cell viability, whilst poorly internalised **18**HC also did not reduce cancer cell viability despite apparently avoiding endosomal trapping or aggregation (Figure4B). However, conjugation of both TAT_{48-57} and the SV40 NLS to **20** led to significant reduction in the viability of both MCF-7 and ZR75-1 breast cancer cells. This suggests that cell and nuclear penetration were the limiting factors for AP-1 inhibition by **20** since TAT_{48-57} and NLS appendages alone had no effect on cell viability and non-specific cell lysis was negligible. Thus, we have demonstrated that once sufficiently internalised into the cell nucleus, **20** displays significant inhibition of AP-1-driven oncogenesis. Moreover, once internalised the CPP component of the peptide is predicted to expendable, without significant effect on the activity of **20**.

CONCLUSION

The strategy of iterative sequence truncation, coupled with insertion of helix-inducing constraints at appropriate positions, was used to reduce the size of Fos to peptide fragments as antagonists of Fos-Jun coiled coil formation. The first crystal structure of an AP-1 antagonist, a Fos-derived peptide complexed with Jun, was used to design helix-constrained and truncated peptides that similarly bound to Jun. Several rounds of iteration led to peptides **18** and **20,** which were efficient Jun-binding ligands relative to their size and were able to inhibit the Fos–Jun interaction. Compounds **18** and **20** represented compromises between downsizing to a minimal binding sequence and retaining appreciable binding affinity for Jun. Isothermal titration calorimetry measurements revealed that the helix-inducing constraint provided an entropic advantage for binding to Jun relative to analogous unstructured short peptides. Importantly, the cell penetrating peptide $TAT_{48\text{-}57}$ together with the nuclear localisation signal peptide SV40, or alternatively a hydrocarbon (*i→i+4*) helix-constraining linker, enabled substantial cell uptake and delivery of **18** and **20** into the nucleus of cells where AP-1 is active. With these adaptations, compound **20** was able to both enter the nucleus of cancer cells and reduce their proliferation *in vitro* at low μM concentrations. This potency compares favourably with small molecule AP-1 inhibitors such as momordin I (IC_{50} ≈ 30 μM) and T-5524 (IC_{50} ≈ 10 μM) that have reached clinical trials [18, 48]. Compound **20** represents one of few examples to date of a helix-constrained peptide that can modulate a PPI featuring coiled-coil peptides [25, 42]. The approach highlighted here, using helix-inducing constraints to compensate for shortening the sequence of a binding partner in a coiled coil transcription factor, shows considerable promise. Further development of Jun antagonists based on truncating Fos is required to generate useful AP-1 inhibitors suitable for treating cancers featuring AP-1 dysregulation.

METHODS

Circular Dichroism (CD spectra and thermal melts)

Coiled coil stability was analysed as previously described [5] using a Chirascan (Applied Photophysics) instrument, recording ellipticity of homotypic (peptide) or heterotypic (1:1

peptide:Jun stoichiometric mix) samples at a total peptide concentration (P_t) of 150 μM, dissolved in 10 mM potassium phosphate buffer with 100 mM potassium fluoride, pH 7.

Isothermal titration calorimetry (ITC)

Coiled coil interaction thermodynamics were assessed as previously described [5] using a Microcal VP-ITC instrument (GE Healthcare). Jun at 100 μM - 3 mM was injected into peptide homotypic samples at 9 μM – 200 μM in circular dichroism buffer.

SUPPORTING INFORMATION

Peptide characterisation, Peptide synthesis and purification, CD measurements and fitting procedures, ITC measurements and fitting procedures, X-ray crystallography procedures (Table S1), Cell culture and assays, Live Cell Confocal Microscopy, Flow Cytometry, Cell Viability, Peptide haemolytic activity (Table S2), and Supplementary results (Figures S1-5).

AUTHOR CONTRIBUTIONS

D.B. conducted Jun-binding CD and ITC experiments, and synthesized, purified and characterised LIN20 and Jun. S.P. conducted all cell experiments. T.H. and W.K. synthesized, purified and characterised all peptides with and without helix-inducing constraints. N.Z and R.B. crystallized the FosW–Jun complex and determined the crystal structure. D.F. and J.M. directed the research. All authors participated in experimental design, analysis of the data, and writing the paper.

COMPETING FINANTIAL INTERESTS

The authors declare no competing financial interests.

ACKNOWLEDGEMENTS

J.Mason is grateful to Cancer Research UK for a Career Establishment Award (A11738), to the BBSRC for a CASE Studentship (BB/J011290/2) and to the EPSRC for an Overseas Travel

Grant (EP/M001873/2). D.Fairlie thanks the National Health and Medical Research Council of Australia for Senior Principal Research Fellowships (1027369, 1117017) and the Australian Research Council for grants (DP160104442, CE140100011). The authors would like to thank Dr. Christopher G. Ullman for useful discussions.

REFERENCES

1. Hill, T. A.; Shepherd, N. E.; Diness, F.; Fairlie, D. P., Constraining Cyclic Peptides To Mimic Protein Structure Motifs. *Angew. Chem.-Int. Edit.* **2014,** *53*, 13020-13041.
2. O'Neil, K. T.; DeGrado, W. F., A thermodynamic scale for the helix-forming tendencies of the commonly occurring amino acids. *Science* **1990,** *250*, 646-651.
3. Mason, J. M.; Arndt, K. M., Coiled coil domains: stability, specificity, and biological implications. *Chembiochem* **2004,** *5*, 170-176.
4. Grigoryev, Y., Stapled peptide to enter human testing, but affinity questions remain. *Nat. Med.* **2013,** *19*, 120-120.
5. Rao, T.; Ruiz-Gómez, G.; Hill, T. A.; Hoang, H. N.; Fairlie, D. P.; Mason, J. M., Truncated and helix-constrained peptides with high affinity and specificity for the cFos coiled-coil of AP-1. *PLoS One* **2013,** *8*, e59415-e59426.
6. Walensky, L. D.; Kung, A. L.; Escher, I.; Malia, T. J.; Barbuto, S.; Wright, R. D.; Wagner, G.; Verdine, G. L.; Korsmeyer, S. J., Activation of apoptosis in vivo by a hydrocarbon-stapled BH3 helix. *Science* **2004,** *305*, 1466-1470.
7. Madala, P. K.; Tyndall, J. D. A.; Nall, T.; Fairlie, D. P., Update 1 of: Proteases Universally Recognize Beta Strands In Their Active Sites. *Chem. Rev.* **2010,** *110*, PR1-PR31.
8. Bird, G. H.; Madani, N.; Perry, A. F.; Princiotto, A. M.; Supko, J. G.; He, X.; Gavathiotis, E.; Sodroski, J. G.; Walensky, L. D., Hydrocarbon double-stapling remedies the proteolytic instability of a lengthy peptide therapeutic. *Proc. Natl. Acad. Sci. USA* **2010,** *107*, 14093-14098.
9. de Araujo, A. D.; Hoang, H. N.; Kok, W. M.; Diness, F.; Gupta, P.; Hill, T. A.; Driver, R. W.; Price, D. A.; Liras, S.; Fairlie, D. P., Comparative alpha-Helicity of Cyclic Pentapeptides in Water. *Angew. Chem. Int. Ed.* **2014,** *53*, 6965-6969.
10. Bock, J. E.; Gavenonis, J.; Kritzer, J. A., Getting in Shape: Controlling Peptide Bioactivity and Bioavailability Using Conformational Constraints. *ACS Chem. Biol.* **2013,** *8*, 488-499.
11. Angel, P.; Karin, M., The role of Jun, Fos, and the AP-1 complex in cell-proliferation and transformation. *Biochim. Biophys. Acta* **1991,** *1072*, 129-157.
12. Eferl, R.; Wagner, E. F., AP-1: a double-edged sword in tumorigenesis. *Nat. Rev. Cancer* **2003,** *3*, 859-868.
13. Jochum, W.; Passegue, E.; Wagner, E. F., AP-1 in mouse development and tumorigenesis. *Oncogene* **2001,** *20*, 2401-2412.
14. Kouzarides, T.; Ziff, E., The role of the Leucine Zipper in the Fos Jun interaction. *Nature* **1988,** *336*, 646-651.
15. Glover, J. N. M.; Harrison, S. C., Crystal structure of the heterodimeric bZIP transcription factor c-Fos–c-Jun bound to DNA. *Nature* **1995,** *373*, 257-261.
16. Corbi-Verge, C.; Kim, P. M., Motif mediated protein-protein interactions as drug targets. *Cell Commun. Signal.* **2016,** *14*, 12.
17. Ye, N.; Ding, Y.; Wild, C.; Shen, Q.; Zhou, J., Small Molecule Inhibitors Targeting Activator Protein 1 (AP-1). *J. Med. Chem.* **2014,** *57*, 6930-6948.
18. Yap, J. L.; Chauhan, J.; Jung, K.-Y.; Chen, L.; Prochownik, E. V.; Fletcher, S., Small-molecule inhibitors of dimeric transcription factors: Antagonism of protein-protein and protein-DNA interactions. *MedChemComm* **2012,** *3*, 541-551.
19. Lloyd, A.; Yancheva, N.; Wasylyk, B., Transformation suppressor activity of a Jun transcription factor lacking its activation domain. *Nature* **1991,** *352*, 635-638.

20. Brown, P. H.; Alani, R.; Preis, L. H.; Szabo, E.; Birrer, M. J., Suppression of oncogene-induced transformation by a deletion mutant of c-jun. *Oncogene* **1993,** *8*, 877-886.
21. Bains, N. P. S.; Wilce, J. A.; Heuer, K. H.; Tunstall, M.; Mackay, J. P.; Bennett, M. R.; Weiss, A. S.; King, G. F., Zipping up transcription factors: Rational design of anti-Jun and anti-Fos peptides. *Lett. Pept. Sci.* **1997,** *4*, 67-77.
22. Olive, M.; Krylov, D.; Echlin, D. R.; Gardner, K.; Taparowsky, E.; Vinson, C., A dominant negative to activation protein-1 (AP1) that abolishes DNA binding and inhibits oncogenesis. *J. Biol. Chem.* **1997,** *272*, 18586-18594.
23. Brown, P. H.; Chen, T. K.; Birrer, M. J., Mechanism of action of a dominant-negative mutant of c-Jun. *Oncogene* **1994,** *9*, 791-799.
24. Liu, Y. M.; Lu, C. H.; Shen, Q.; Munoz-Medellin, D.; Kim, H.; Brown, P. H., AP-1 blockade in breast cancer cells causes cell cycle arrest by suppressing G1 cyclin expression and reducing cyclin-dependent kinase activity. *Oncogene* **2004,** *23*, 8238-8246.
25. Edwards, A. L.; Meijer, D. H.; Guerra, R. M.; Molenaar, R. J.; Alberta, J. A.; Bernal, F.; Bird, G. H.; Stiles, C. D.; Walensky, L. D., Challenges in Targeting a Basic Helix-Loop-Helix Transcription Factor with Hydrocarbon-Stapled Peptides. *ACS Chem. Biol.* **2016,** *11*, 3146-3153.
26. Mason, J. M.; Schmitz, M. A.; Muller, K.; Arndt, K. M., Semirational design of Jun-Fos coiled coils with increased affinity: Universal implications for leucine zipper prediction and design. *Proc. Natl. Acad. Sci. USA* **2006,** *103*, 8989-8994.
27. Worrall, J. A.; Mason, J. M., Thermodynamic analysis of Jun-Fos coiled coil peptide antagonists. *FEBS J* **2011,** *278*, 663-72.
28. Acharya, A.; Rishi, V.; Vinson, C., Stability of 100 homo and heterotypic coiled-coil ***a–a'*** pairs for ten amino acids (A, L, I, V, N, K, S, T, E, and R). *Biochemistry* **2006,** *45*, 11324-11332.
29. O'Shea, E. K.; Klemm, J. D.; Kim, P. S.; Alber, T., X-ray structure of the GCN4 leucine zipper, a 2-stranded, parallel coiled coil. *Science* **1991,** *254*, 539-544.
30. Halazonetis, T. D.; Georgopoulos, K.; Greenberg, M. E.; Leder, P., c-Jun dimerizes with itself and with c-Fos, forming complexes of different DNA-binding affinities. *Cell* **1988,** *55*, 917-924.
31. Resh, M. D., Fatty acylation of proteins: new insights into membrane targeting of myristoylated and palmitoylated proteins. *Biochim. Biophys. Acta-Mol. Cell Res.* **1999,** *1451*, 1-16.
32. Debaisieux, S.; Rayne, F.; Yezid, H.; Beaumelle, B., The Ins and Outs of HIV-1 Tat. *Traffic* **2012,** *13*, 355-363.
33. Lanford, R. E.; Kanda, P.; Kennedy, R. C., Induction of nuclear transport with a synthetic peptide homologous to the SV40 T-antigen transport signal. *Cell* **1986,** *46*, 575-582.
34. Liu, Y. M.; Ludes-Meyers, J.; Zhang, Y.; Munoz-Medellin, D.; Kim, H. T.; Lu, C. H.; Ge, G. Q.; Schiff, R.; Hilsenbeck, S. G.; Osborne, C. K.; Brown, P. H., Inhibition of AP-1 transcription factor causes blockade of multiple signal transduction pathways and inhibits breast cancer growth. *Oncogene* **2002,** *21*, 7680-7689.
35. Fu, J.; Cheng, L.; Wang, Y.; Yuan, P.; Xu, X. J.; Ding, L. H.; Zhang, H.; Jiang, K.; Song, H. F.; Chen, Z. W.; Ye, Q. N., The RNA-binding protein RBPMS1 represses AP-1 signaling and regulates breast cancer cell proliferation and migration. *Biochim. Biophys. Acta-Mol. Cell Res.* **2015,** *1853*, 1-13.
36. Zimm, B. H.; Bragg, J. K., Theory of the phase transition between helix and random coil in polypeptide chains. *J. Chem. Phys.* **1959,** *31*, 526-535.

37. Dragan, A. I.; Privalov, P. L., Unfolding of a leucine zipper is not a simple two-state transition. *J. Mol. Biol.* **2002,** *321*, 891-908.
38. Mason, J. M.; Hagemann, U. B.; Arndt, K. M., Improved stability of the Jun-Fos Activator Protein-1 coiled coil motif: A stopped-flow circular dichroism kinetic analysis. *J. Biol. Chem.* **2007,** *282*, 23015-23024.
39. Harrison, R. S.; Shepherd, N. E.; Hoang, H. N.; Ruiz-Gomez, G.; Hill, T. A.; Driver, R. W.; Desai, V. S.; Young, P. R.; Abbenante, G.; Fairlie, D. P., Downsizing human, bacterial, and viral proteins to short water-stable alpha helices that maintain biological potency. *Proc. Natl. Acad. Sci. U. S. A.* **2010,** *107*, 11686-11691.
40. Crick, F. H. C., The Packing of α-Helices: Simple Coiled-Coils. *Acta Crystallogr.* **1953,** *6*, 689-697.
41. Pauling, L.; Corey, R. B.; Branson, H. R., The structure of proteins; two hydrogen-bonded helical configurations of the polypeptide chain. *Proc. Natl. Acad. Sci. U. S. A.* **1951,** *37*, 205-211.
42. Bird, G. H.; Gavathiotis, E.; LaBelle, J. L.; Katz, S. G.; Walensky, L. D., Distinct BimBH3 (BimSAHB) Stapled Peptides for Structural and Cellular Studies. *ACS Chem. Biol.* **2014,** *9*, 831-837.
43. Duchardt, F.; Fotin-Mleczek, M.; Schwarz, H.; Fischer, R.; Brock, R., A comprehensive model for the cellular uptake of cationic cell-penetrating peptides. *Traffic* **2007,** *8*, 848-866.
44. Chen, T. K.; Smith, L. M.; Gebhardt, D. K.; Birrer, M. J.; Brown, P. H., Activation and inhibition of the AP-1 complex in human breast cancer cells. *Mol. Carcinog.* **1996,** *15*, 215-226.
45. Jiao, X. M.; Katiyar, S.; Willmarth, N. E.; Liu, M. R.; Ma, X. J.; Flomenberg, N.; Lisanti, M. P.; Pestell, R. G., c-Jun Induces Mammary Epithelial Cellular Invasion and Breast Cancer Stem Cell Expansion. *J. Biol. Chem.* **2010,** *285*, 8218-8226.
46. Smith, L. M.; Wise, S. C.; Hendricks, D. T.; Sabichi, A. L.; Bos, T.; Reddy, P.; Brown, P. H.; Birrer, M. J., cJun overexpression in MCF-7 breast cancer cells produces a tumorigenic, invasive and hormone resistant phenotype. *Oncogene* **1999,** *18*, 6063-6070.
47. Kousidou, O. C.; Berdiaki, A.; Kletsas, D.; Zafiropoulos, A.; Theocharis, A. D.; Tzanakakis, G. N.; Karamanos, N. K., Estradiol-estrogen receptor: A key interplay of the expression of syndecan-2 and metalloproteinase-9 in breast cancer cells. *Mol. Oncol.* **2008,** *2*, 223-232.
48. Ye, N.; Ding, Y.; Wild, C.; Shen, Q.; Zhou, J., Small Molecule Inhibitors Targeting Activator Protein-1 (AP-1). *J. Med. Chem.* **2014,** *57*, 6930-6948.
49. Crooks, R. O.; Rao, T.; Mason, J. M., Truncation, randomization, and selection: generation of a reduced length c-Jun antagonist that retains high interaction stability. *J. Biol. Chem.* **2011,** *286*, 29470-29479.

FIGURE LEGENDS

Figure 1: Crystal structure of the FosW–Jun coiled coil. Top left: FosW and Jun sequences. Stabilising interhelical hydrophobic interactions (***a***$_i$-***a'***$_i$ and ***d***$_i$-***d'***$_i$) are shown as vertical lines and specificity-conferring interhelical electrostatic interactions (***g***$_i$-***e'***$_{i+7}$ and ***e***$_i$-***g'***$_{i-7}$), are shown as green arrows. Heptad register is shown in italics above FosW sequence. **Left:** Helical wheel diagram of FosW (showing residues selected from Fos library in red) in interaction with Jun, including interhelical interactions between ***e*** and ***g*** residues (green arrows). Adapted from source [26]. **Right:** Crystal structure of the FosW–cJun coiled coil at 2.3 Å resolution. FosW is shown as a red helix, with cJun shown as a green helix. Side chains for ***a***, ***d***, ***e*** and ***g*** residues only are shown, using CPK colouring. Helices run from N-terminus (top) to C-terminus (bottom). See Table S1 for crystallisation and structure solving parameters. Model rendered with the PyMOL Molecular Graphics System, Version 1.8 Schrödinger, LLC.

Figure 2: Helix-constrained and truncated Fos peptides. Design template FosW sequence in bold. Heptad register ***a***-***g*** through each heptad of FosW in italics. Helix constraints between lysine and aspartate are shown in blue. Standard single letter amino acid code except Pal = palmitic acid, TAT_{48-57} = First 10 residues of the HIV-1 Tat peptide [32], NLS = the monopartite SV40 large T-antigen nuclear localisation signal [33], Ac- = N-terminal acetyl modification, -NH_2 = C-terminal amine, X = (S)α-(2'-pentenyl)alanine. Dissociation constants (K_d) measured by isothermal titration calorimetry (ITC), and fractional helicites calculated from ellipticity measured by circular dichroism spectroscopy (CD) using Equation 4 (see Supporting Information) [49]. Constraint of all heptads except Heptad 3 generated full length peptides (minus AS and GAP capping motifs) with similar dissociation constants to that of FosW but improved helicity, whist addition of a second constraint was generally effective in inducing further increased helicity, and even lower dissociation constants. Truncations from N- and C-termini were effective if combined with optimal positioning of constraints. ITC experiments not performed because binding measured by CD was negligible are labelled "ND" ("not determined"). ITC experiments that generated binding too weak for accurate fitting are labelled "NF" ("not fit").

Figure 3: Peptide 20 binds Jun and tolerates cell penetrating peptide appendages. Thermal denaturation profiles (A, C) and isothermal titration calorimetry (B, D) of peptide:Jun

mixtures compared to FosW–Jun. (A, C) Thermal melt data is reported as change in mean residue ellipticity (MRE; units deg cm^2/dmol), as a function of circular dichroism ellipticity at 222 nm with temperature. Blue: peptide alone, red: equimolar mix of peptide with Jun, grey: average of Jun and peptide alone (representing non-interaction), black: Jun alone. (B, D) Raw isotherms (top panels) and fitted data (bottom panels) (both baseline corrected) for peptides with Jun compared to FosW. Injection enthalpies for the buffer into buffer control (blue text label) on the NLS-TAT_{48-57} plot are translated by -0.05 µcal/sec for clarity relative to those for Jun into NLS-TAT_{48-57}. In shortened peptide **20**, constraints induce high helicity despite truncation, and this peptide retains significant binding free energy of FosW despite loss of interaction contacts due to entropic stabilisation. In contrast, linear counterpart LIN20 displays poor helicity and 27-fold reduced affinity for Jun compared to **20**.

Figure 4: Intracellular delivery of 18 and 20 alone versus with appended cationic cell penetrating peptides. (A) Peptides were incubated at 10 µM for one or six hours at 37 °C in serum free media on MCF-7 cells. Quantitation by flow cytometry with fluorescence intensity calculated from live single cells. Data shown are means (+ SEM) of four independent repeats (B) Live cell confocal microscopy of MCF-7 cells. Peptides were incubated at 10 µM for 6 h at 37 °C in serum free media. Nuclei were counterstained with Hoechst. Scale bar = 20 µm. Viability of MCF-7 (C) and ZR75-1 (D) breast cancer cells after a 96-hour incubation with the indicated peptide concentrations in complete medium. Data is normalised to vehicle (DMSO) control. Data shown are means (+ SEM) of three independent experiments. * $P < 0.05$, **** $P < 0.0001$ (Student's T-test) decrease relative to DMSO control.

Table 1: Thermodynamic parameters for Jun interaction with lactam constrained FosW derivative peptides. Data from CD and ITC measurements (2 s.f.). θ is raw CD ellipticity (mdeg). Equations for fractional helicity and the Gibbs-Helmholtz equation, from which TΔS is calculated as ΔH – ΔG, are provided in the Supplementary Information. FosW–Jun CD values from Worrall and Mason (2011). CD values are taken from representative single measurements, which are typically reproducible in biological replicates to ± 1 °C for T_m, within 5 % for fractional helicity and 222:208 ratio ($\theta_{222}/_{208}$), and within 10 % for K_d and ΔG (data not shown). ITC values are the arithmetic mean of at least two independent titrations ± SDs, except values from Worrall and Mason (2011) indicated with an asterisk and values

for **20**-TAT_{48-57} and **20**-NLS-TAT_{48-57} (single titrations and fitting errors). CD and ITC data generally agree to within 15 % for ΔG and an order of magnitude for K_d. ITC experiments not performed because binding measured by CD was negligible are labelled “ND” (“not determined”). CD or ITC experiments that generated binding too weak for accurate fitting are labelled “NF” (“not fit”).

Complex	T_m (°C) (CD)	Peptide–cJun Fractional Helicity (%) (CD)	$K_{d(20°C)}$ (nM) (CD)	$\Delta G_{(20°C)}$ (kcal/mol) (CD)	$K_{d(20°C)}$ (nM) (ITC)	N interaction stoichiometry (ITC)	$\Delta G_{(20°C)}$ (kcal/mol) (ITC)	$\Delta H_{(20°C)}$ (kcal/mol) (ITC)	$T\Delta S_{(20°C)}$ (kcal/mol) (ITC)	Peptide–cJun $\Theta_{222}/_{208}$ (20°C) (CD)
cFos–cJun*	16	28	320,000	-5.5	27,000	1.1 ± 0.01	-6.1 ± 0.39	-0.82 ± 0.36	5.3 ± 0.53	0.75
FosW–cJun	63	37	4.0	-11	39 ± 11	0.99 ± 0.08	-9.9 ± 0.16	-10 ± 0.42	-0.46 ± 0.46	1.0
1–cJun	65	44	0.51	-13	9.6 ± 5.7	0.92 ± 0.42	-11 ± 0.35	-12 ± 0.62	-1.1 ± 0.67	0.98
2–cJun	60	62	19	-10	16 ± 4.7	0.95 ± 0.03	-10 ± 0.17	-13 ± 0.30	-3.0 ± 0.41	1.0
3–cJun	NF	29	NF	NF	ND	ND	ND	ND	ND	0.70
4–cJun	63	60	33	-10	40 ± 11	0.86 ± 0.10	-9.9 ± 0.16	-14 ± 0.33	-3.9 ± 0.44	1.0
5–cJun	67	74	2.8	-12	29 ± 19	1.1 ± 0.25	-10 ± 0.39	-13 ± 0.80	-2.6 ± 1.4	1.1
6–cJun	66	56	2.4	-12	19 ± 6.6	0.57 ± 0.01	-10 ± 0.20	-16 ± 1.0	-6.0 ± 1.1	1.0
7–cJun	71	73	3.0	-11	8.6 ± 1.8	0.99 ± 0.01	-11 ± 0.12	-14 ± 1.1	-2.8 ± 1.2	1.1
8–cJun	71	75	0.54	-12	9.9 ± 4.0	0.77 ± 0.14	-11 ± 0.23	-12 ± 1.5	-1.5 ± 1.6	1.0
9–cJun	68	77	1.6	-12	11 ± 5.5	0.60 ± 0.11	-11 ± 0.30	-14 ± 1.5	-2.9 ± 1.7	1.0
10–cJun	NF	34	NF	NF	ND	ND	ND	ND	ND	0.82
11–cJun	NF	14	NF	NF	ND	ND	ND	ND	ND	0.61
12–cJun	NF	25	NF	NF	ND	ND	ND	ND	ND	0.78
13–cJun	NF	27	NF	NF	ND	ND	ND	ND	ND	0.79
14–cJun	44	44	1100	-8.0	2200 ± 450	0.75 ± 0.29	-7.6 ± 0.12	-13 ± 1.0	-5.7 ± 1.0	0.97
15–cJun	48	62	1100	-8.0	1000 ± 560	0.48 ± 0.15	-8.0 ± 0.32	-13 ± 0.85	-5.2 ± 1.1	1.0
16–cJun	38	49	6000	-7.0	ND	ND	ND	ND	ND	1.0
17–cJun	19	44	100,000	-5.4	ND	ND	ND	ND	ND	0.85
18–cJun	60	69	18	-10	56 ± 14	0.71 ± 0.04	-9.7 ± 0.15	-14 ± 0.35	-4.0 ± 0.36	1.0
19–cJun	63	60	8.3	-11	110 ± 50	0.62 ± 0.12	-9.4 ± 0.28	-10 ± 0.54	-1.1 ± 0.53	0.98
20–cJun	47	62	2000	-7.7	2000 ± 420	0.67 ± 0.08	-7.6 ± 0.12	-4.9 ± 0.37	2.8 ± 0.40	0.99
LIN**20**–cJun	NF	39	NF	NF	55,000 ± 9700	1.4 ± 0.07	-5.7 ± 0.10	-6.0 ± 0.38	-0.25 ± 0.38	0.81
LIN**20**-TAT_{48-57}–cJun	42	59	3500	-7.3	ND	ND	ND	ND	ND	0.91
Pal-**20**–cJun	NF	28	NF	NF	ND	ND	ND	ND	ND	0.82
20-TAT_{48-57}–cJun	53	70	1100	-8.0	5600 ± 380	1.1 ± 0.01	-7.1 ± 0.04	-5.3 ± 0.05	1.8 ± 0.06	0.95
20-NLS-TAT_{48-57}–cJun	43	39	3100	-7.4	7600 ± 460	0.59 ± 0.00	-6.9 ± 0.04	-5.5 ± 0.06	1.3 ± 0.07	0.79
NLS-TAT_{48-57}–cJun	NF	11	NF	NF	NF	NF	NF	NF	NF	0.33
18HC–cJun	48	44	69	-9.6	320 ± 50	0.70 ± 0.01	-8.7 ± 0.09	-6.6 ± 0.40	2.1 ± 0.50	0.89
20HC–cJun	33	35	3300	-7.4	15,000 ± 2400	1.1 ± 0.23	-6.5 ± 0.09	-4.5 ± 0.40	2.0 ± 0.41	0.81

```
abcdefg abcdefg abcdefg abcdefg abcd
LDELQAE IEQLEER NYALRKE IEDLQKQ LEKL  FosW
|   |     |   |     |   |     |   |     |   |
IARLEEK VKTLKAQ NYELAST ANMLREQ VAQL  cJun
```

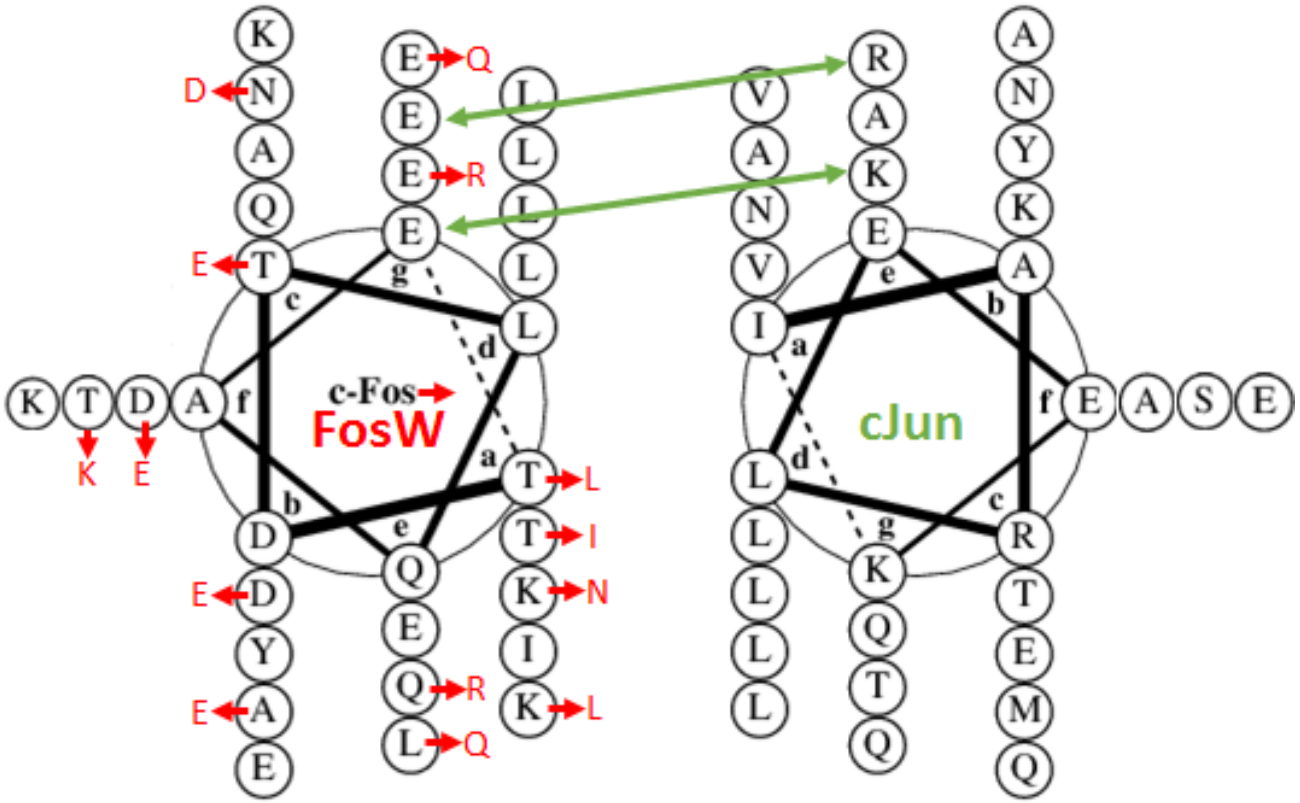

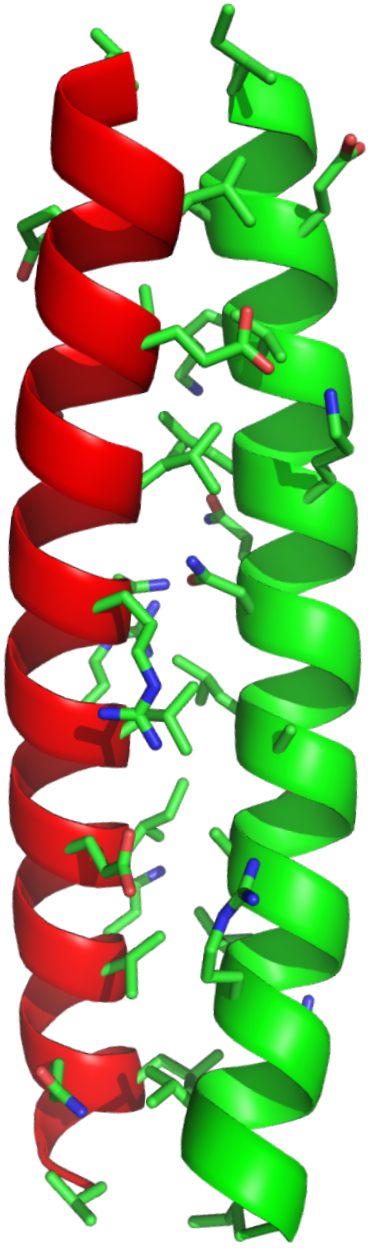

	Heptad 1 a b c d e f g	Heptad 2 a b c d e f g	Heptad 3 a b c d e f g	Heptad 4 a b c d e f g	Heptad 4.5 a b c d	Truncation vs. FosW	Peptide–cJun $K_{d(20°C)}$ (nM) (ITC)	Peptide Helicity (%) (CD)	Peptide–cJun Helicity (%) (CD)
FosW:	AS**LDELQAE**	**IEQLEER**	**NYALRKE**	**IEDLQKQ**	**LEKL**GAP	N/A	39 ± 11	41	37
1	Ac-LDELQAE	IEQLEER	NYALRKE	IEDLQKQ	LEDL-NH_2	NΔ2 CΔ3	9.6 ± 5.7	44	44
2	Ac-LDELQAE	IEQLEER	NYALRKE	IKDLQDQ	LEKL-NH_2	NΔ2 CΔ3	16 ± 4.7	62	62
3	Ac-LDELQAE	IEQLEER	NKALRDE	IEDLQKQ	LEKL-NH_2	NΔ2 CΔ3	ND	40	29
4	Ac-LDELQAE	IKQLEDR	NYALRKE	IEDLQKQ	LEKL-NH_2	NΔ2 CΔ3	40 ± 11	59	60
5	Ac-LKELQDE	IEQLEER	NYALRKE	IEDLQKQ	LEKL-NH_2	NΔ2 CΔ3	29 ± 19	79	74
6	Ac-LDELQAE	IEQLEER	NYALRKE	IEDLQKQ	LEDL-NH_2	NΔ2 CΔ3	19 ± 6.6	53	56
7	Ac-LDELQAE	IEQLEKR	NYDLRKE	IEDLQKQ	LEDL-NH_2	NΔ2 CΔ3	8.6 ± 1.8	85	73
8	Ac-LDELQKE	IEDLEER	NYALRKE	IEDLQKQ	LEDL-NH_2	NΔ2 CΔ3	9.9 ± 4.0	78	75
9	Ac-LKELQDE	IEQLEER	NYALRKE	IEDLQKQ	LEDL-NH_2	NΔ2 CΔ3	11 ± 5.5	82	77
10		Ac-LEKR	NYDLRKE	IEDLQKQ	LEDL-NH_2	NΔ12 CΔ3	ND	64	34
11		Ac-LEKR	NYDLRKE	IEDLQKQ	LEDL-NH_2	NΔ12 CΔ3	ND	17	14
12	Ac-LQKE	IEDLEER	NYALRKE	IEDL-NH_2		NΔ5 CΔ10	ND	28	25
13	Ac-LQKE	IEDLEKR	NYDLRKE	IEDL-NH_2		NΔ5 CΔ10	ND	38	27
14	Ac-LKELQDE	IEQLEER	NYALRKE	IEDL-NH_2		NΔ2 CΔ10	2200 ± 450	39	44
15	Ac-LKELQDE	IEQLEKR	NYDLRKE	IEDL-NH_2		NΔ2 CΔ10	1000 ± 560	65	62
16	Ac-LDELQAE	IEQLEKR	NYDLRKE	IEDL-NH_2		NΔ2 CΔ10	ND	48	49
17		Ac-IEQLEKR	NYDLRKE	IEDLQKQ	L-NH_2	NΔ9 CΔ6	ND	67	44
18	Ac-LKAE	IDQLEER	NYALRKE	IEDLQKQ	LEDL-NH_2	NΔ5 CΔ3	56 ± 14	72	69
19	Ac-LQAE	IKQLEDR	NYALRKE	IEDLQKQ	LEDL-NH_2	NΔ5 CΔ3	110 ± 50	64	60
20		Ac-IKQLEDR	NYALRKE	IEDLQKQ	LEDL-NH_2	NΔ9 CΔ3	2000 ± 420	85	62
LIN20		Ac-IKQLEDR	NYALRKE	IEDLQKQ	LEDL-NH_2	NΔ9 CΔ3	55,000 ± 9700	50	39
LIN20-TAT_{48-57}		Ac-IKQLEDR	NYALRKE	IEDLQKQ	LEDL RKKRRQRRR-NH_2	NΔ9 CΔ3	ND	66	59
Pal-**20**		Pal-IKQLEDR	NYALRKE	IEDLQKQ	LEDL-NH_2	NΔ9 CΔ3	ND	28	28
20-TAT_{48-57}		Ac-IKQLEDR	NYALRKE	IEDLQKQ	LEDL RKKRRQRRR-NH_2	NΔ9 CΔ3	5600 ± 380	96	70
20-NLS-TAT_{48-57}		Ac-IKQLEDR	NYALRKE	IEDLQKQ	LEDL PKKKRKVYGRKKRRQRRR-NH_2	NΔ9 CΔ3	7600 ± 460	46	39
NLS-TAT_{48-57}					Ac-PKKKRKVYGRKKRRQRRR-NH_2	N/A	NF	0	11
18HC	Ac-LXAE	IXQLEER	NYALRKE	IEDLQXQ	LEXL-NH_2	NΔ9 CΔ3	320 ± 50	40	44
20HC		Ac-IXQLEXR	NYALRKE	IEDLQXQ	LEXL-NH_2	NΔ9 CΔ3	15,000 ± 2400	49	35

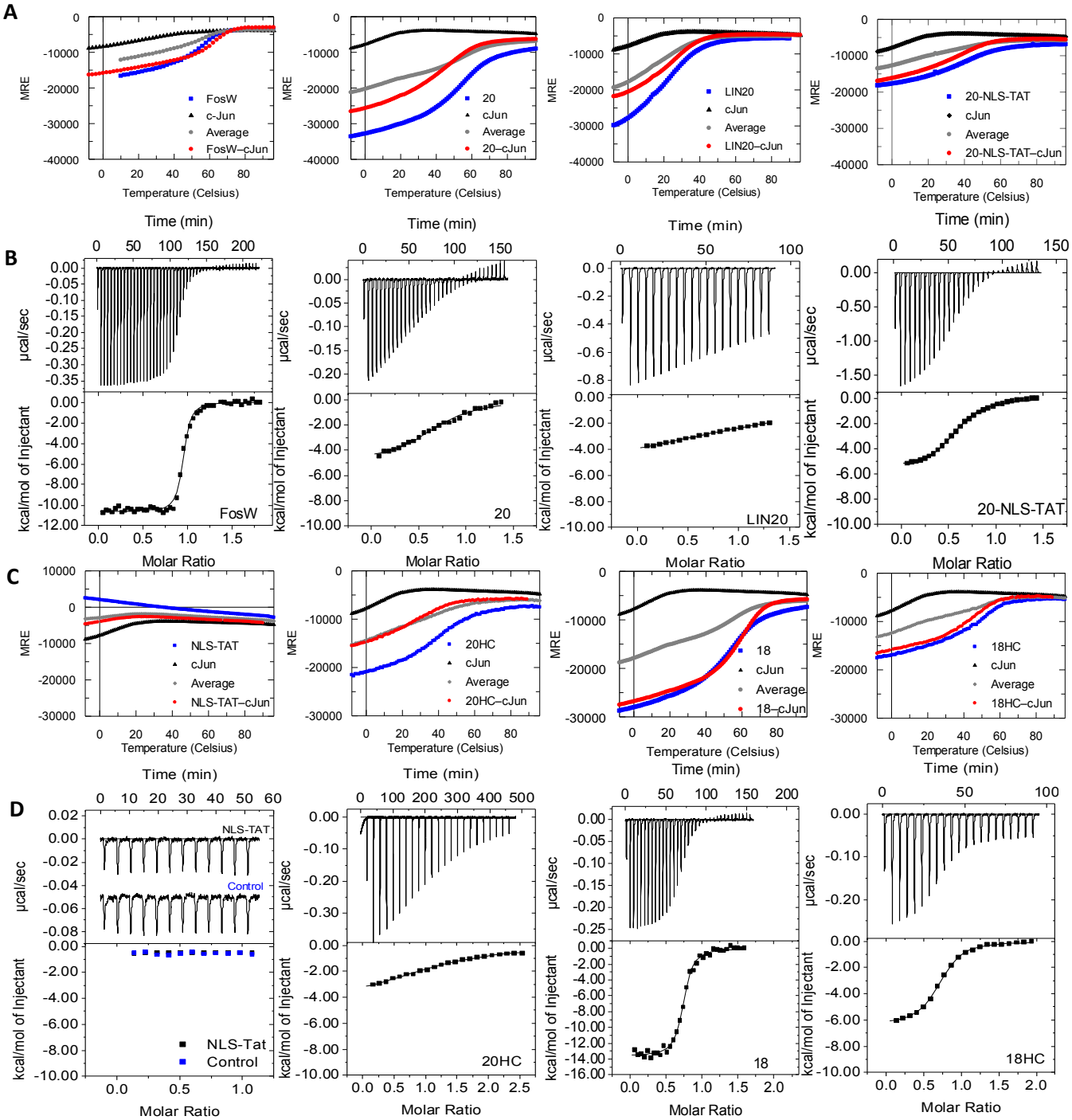
A
MRE
Temperature (Celsius)
FosW
c-Jun
Average
FosW–cJun
20
cJun
Average
20–cJun
LIN20
cJun
Average
LIN20–cJun
20-NLS-TAT
cJun
Average
20-NLS-TAT–cJun
B
Time (min)
µcal/sec
kcal/mol of Injectant
Molar Ratio
FosW
20
LIN20
20-NLS-TAT
C
NLS-TAT
cJun
Average
NLS-TAT–cJun
20HC
cJun
Average
20HC–cJun
18
cJun
Average
18–cJun
18HC
cJun
Average
18HC–cJun
D
NLS-TAT
Control
NLS-Tat
Control
20HC
18
18HC

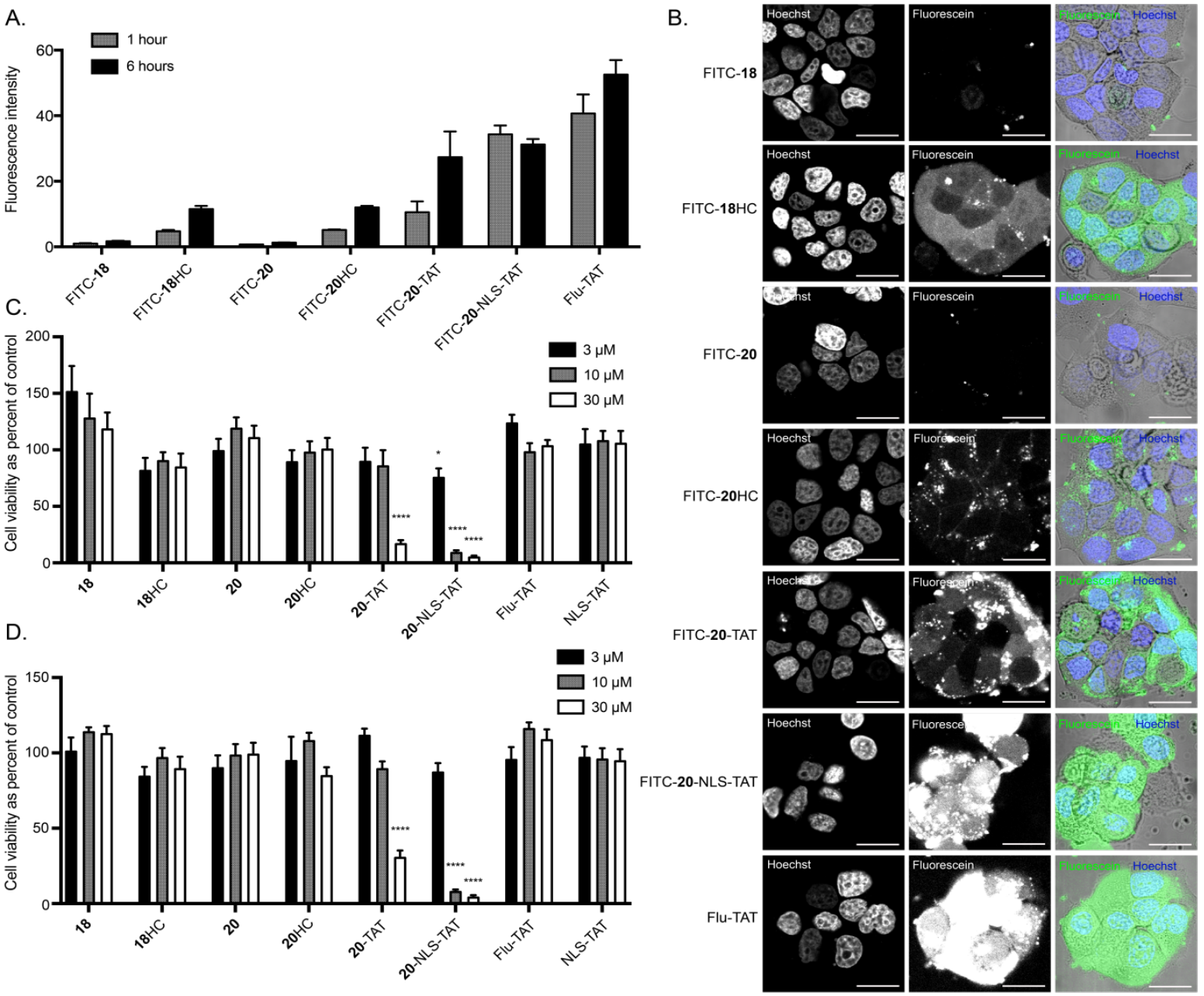
A.
1 hour
6 hours
Fluorescence intensity
60
40
20
0
FITC-18
FITC-18HC
FITC-20
FITC-20HC
FITC-20-TAT
FITC-20-NLS-TAT
Flu-TAT
B.
FITC-18
FITC-18HC
FITC-20
FITC-20HC
FITC-20-TAT
FITC-20-NLS-TAT
Flu-TAT
Hoechst
Fluorescein
C.
Cell viability as percent of control
200
150
100
50
0
3 µM
10 µM
30 µM
18
18HC
20
20HC
20-TAT
20-NLS-TAT
Flu-TAT
NLS-TAT
D.
Cell viability as percent of control
150
100
50
0
3 µM
10 µM
30 µM
18
18HC
20
20HC
20-TAT
20-NLS-TAT
Flu-TAT
NLS-TAT